NACA

RESEARCH MEMORANDUM

PRELIMINARY INVESTIGATION OF THE EFFECTS OF SEVERAL

SEEKER-NOSE CONFIGURATIONS ON THE LONGITUDINAL

CHARACTERISTICS OF A CANARD-TYPE MISSILE

AT A MACH NUMBER OF 1.60

By A. Warner Robins

Langley Aeronautical Laboratory
Langley Field, Va.

NATIONAL ADVISORY COMMITTEE
FOR AERONAUTICS

WASHINGTON
October 30, 1953

NACA RM L53I18

NATIONAL ADVISORY COMMITTEE FOR AERONAUTICS

RESEARCH MEMORANDUM

PRELIMINARY INVESTIGATION OF THE EFFECTS OF SEVERAL

SEEKER-NOSE CONFIGURATIONS ON THE LONGITUDINAL

CHARACTERISTICS OF A CANARD-TYPE MISSILE

AT A MACH NUMBER OF 1.60

By A. Warner Robins

SUMMARY

An investigation has been conducted to determine the effect of several seeker-nose configurations on the static longitudinal stability, the canard control characteristics, and lift and drag at a Mach number of 1.60 of a canard-type ram-jet missile having 70° delta canard control surfaces and 70° delta wings. The angle of attack ranged from about -4° to about 14.5°, and the Reynolds number based on wing mean aerodynamic chord was 3.83×10^6.

The test results indicate that, with the exception of a model with a cruciform nose shape, the configurations tested exhibited no significant difference in either static longitudinal stability or horizontal-canard control effectiveness.

Horizontal-canard hinge-moment data were obtained for five of the nose shapes tested and indicated that the spike-nose configurations tended to produce larger hinge moments, this effect being more pronounced in the case of the cone spike. The substitution of the conical or slotted-cone noses for the parabolic nose had little effect on the horizontal-canard hinge moments.

All configurations tested showed less drag in the lower angle-of-attack range than the model with the spherical nose.

INTRODUCTION

The use of seeker-type guidance systems in missiles usually requires the use of a relatively blunt fuselage nose shape in order to accommodate

the seeker "eye" with a relatively unobstructed view forward. Inasmuch as the drag with a large degree of bluntness is considerable, it is important to determine how this drag can be reduced without seriously impairing the guidance system.

At present, much data are available on the effect of spikes on the zero-angle-of-attack flow at supersonic speeds about blunt bodies of revolution (refs. 1 to 6) and of the drag of bodies with various nose shapes at supersonic speeds (refs. 6 to 8). There are little data available, however, which might be useful in the design of optical seeker noses showing the effects of nose shape on the longitudinal stability and control and drag of a model at angles of attack. It is the purpose of this investigation to determine some of the effects at a Mach number of 1.60 of several nose shapes on the longitudinal characteristics at angles of attack of a model of a canard-type ram-jet missile incorporating an optical seeker. The present investigation is in insufficient detail to amplify the results with an explanation of the related flow phenomena.

Much information on the aerodynamic characteristics including longitudinal and lateral stability and control characteristics at a Mach number of 1.60 is available for this missile with a parabolic nose in reference 9. Reference 10 presents the aerodynamics of the missile with various combinations of components.

SYMBOLS

The longitudinal stability-axis system is shown in figure 1. The reference center of gravity was located at -19.5 percent of wing mean aerodynamic chord.

C_L lift coefficient, $-Z/qS$

C_D drag coefficient, $-X/qS$

C_m pitching-moment coefficient, $M'/qS\bar{c}$

C_{h_H} horizontal-canard hinge-moment coefficient, $H_H/qS_H\bar{c}_H$

Z force along Z-axis

X force along X-axis

M' moment about Y-axis

H_H moment about horizontal-canard hinge axis

S_H exposed area of horizontal canard

S total wing area

q free-stream dynamic pressure, $1/2\rho V^2$

ρ free-stream density

V free-stream velocity

$\bar{c}$ wing mean aerodynamic chord

$\bar{c}_H$ horizontal-canard mean aerodynamic chord

M Mach number

α angle of attack, deg

δ_H horizontal-canard deflection, deg

C_{L_α} slope of lift curve

APPARATUS AND MODELS

Basic Model

A canard-type ram-jet missile model having 70° delta forward-control surfaces and 70° delta wings with tip ailerons was used. The ram-jet nacelles were pylon-mounted in the plane of fixed vertical-canard surfaces above and below the fuselage at 90° to the wing plane. Figure 2 shows a three-view drawing of the basic model with the parabolic nose. A photograph of the model, disassembled to show its main components, is shown in figure 3. Table I presents the geometric characteristics of the model, the body coordinates of which are given in table II. Details of the canard control surfaces and wing appear in figure 4. Table III shows nacelle details.

The model was sting-supported as shown in figure 5 and was fitted with a six-component strain-gage balance housed within the fuselage. A small electric motor located forward of the balance actuated a mechanism which provided that the incidence angle of the horizontal-canard surfaces

be remotely controlled. An individual strain-gage balance was used to measure the hinge moments of the horizontal-canard surface.

Nose Shapes

A drawing of the several nose shapes appears in figure 6. The nose parting line is shown in figure 2. Figure 7 is a photograph of all the nose shapes tested.

Parabolic nose.- The parabolic nose, the coordinates of which are given in figure 6, is included only for purposes of comparison.

Spherical nose.- The spherical nose was considered to represent approximately the lens of the seeker system and would therefore be the best, optically, of the nose series. No changes in the model were made behind the nose-body intersection. The ratio of nose radius to maximum body radius was 0.6, approximately.

Conical nose.- The 30° conical nose was considered (ref. 11) to be the minimum-apex-angle translucent cone which could be tolerated optically for seeker use.

30° slotted cone.- The 30° slotted cone, the details of which are shown in figure 6, is composed of a hollow cone from which approximately half of the surface area has been removed in longitudinal strips. Reference 2 includes tests of the slotted-cone nose shape, as well as various modifications of it. This nose shape was designed in an attempt to retain, at high angles of attack, the low-angle-of-attack aerodynamic characteristics of the nose spike by fixing the associated dead-air region (refs. 3 and 4).

30° plain spike.- For spherical nose shapes, considerable drag reduction has been indicated with the use of a spike protruding ahead of the body. The spike tested was somewhat shorter than optimum zero-angle-of-attack spike length (refs. 3 to 5), since it was felt that the long dead-air region associated with the longer spike would be more sensitive to angle of attack. The 30° spike had its apex at the same location as the cruciform, conical, and slotted-cone noses.

30° cone spike.- The 30° cone spike differed from the plain spike only in having a longer conical section which terminated as a shoulder twice the spike diameter. This spike was designed in an attempt to maintain the approximately conical dead-air region at higher angles of attack than the plain spike.

30° cruciform nose.- The cruciform nose, which would be optically good, was an attempt to effect a drag reduction in much the same manner

as the spike configurations and to further aid in fixing the associated dead-air region at angles of attack.

TESTS

Test Conditions

The test conditions were:

Mach number 1.60
Reynolds number, based on wing mean aerodynamic chord . . . 3.83×10^6
Stagnation pressure, atm 1.0
Stagnation temperature, $^{\circ}F$ 110
Stagnation dew point, $^{\circ}F$ . . . . <-25

The latest calibration of the tunnel test section indicates that the magnitude of the Mach number variation is ±0.01 and that the variation of the flow angle in both the horizontal and vertical planes is about $\pm0.1^{\circ}$.

Corrections and Accuracy

The deflections of the balance under load were applied to the angles of attack so that the estimated accuracy of the angle of attack was $\pm0.1^{\circ}$ In the reduction of data, no corrections were made for flow variations in the test section. The base pressure was measured and the chord-force data were corrected to correspond to a base pressure equal to free-stream static pressure.

The estimated errors in the force data were:

C_L . . . . ±0.004
C_D . . . . ±0.0023
C_m . . . . ±0.0004
C_{h_H} . . . . ±0.0005
δ_H . . . . ±0.1

RESULTS AND DISCUSSION

The results are presented in figures 8 to 11 showing pitching-moment coefficient, horizontal-canard hinge-moment coefficient, drag coefficient, and angle of attack plotted against lift coefficient, respectively.

Figure 8, which shows the variation of pitching-moment coefficient with lift coefficient for horizontal-canard-control deflections of 0°, 4°, 8°, and 12°, indicates that no appreciable change results from the installation of any of the nose configurations except the cruciform shape. The missile with the cruciform nose shape produced higher pitching moments as greater lift coefficients and canard deflections were experienced, indicating that this nose shape behaved as a lifting surface. The fact that the pitching-moment-coefficient curves were substantially the same for the remaining nose shapes is noteworthy, considering the large differences in flow fields at the noses. Reference 9 presents in greater detail the static longitudinal stability characteristics of the missile with the parabolic nose.

Figure 9 shows the horizontal-canard hinge-moment coefficients for four of the seeker-nose shapes compared to those for the parabolic nose. Hinge moments for the configurations with the spherical and cruciform nose shapes were not measured. The spike-nose configurations tended to produce larger negative moments as canard-control angles were increased, this effect being more pronounced in the case of the cone spike. The substitution of the conical or slotted-cone noses for the parabolic nose had little effect on the horizontal-canard hinge moments. A comparison of experimental and theoretical horizontal-canard hinge moments at zero angle of attack for the missile with the parabolic nose is presented in reference 9.

Since the data were obtained for a complete configuration in which approximately 60 percent of the total drag is attributed to the nacelles and nacelle struts (ref. 10), the drag differences for the model with various nose shapes are generally small compared to total drag. As previously indicated in the section "Corrections and Accuracy," it appears that the accuracy of the chord-force measurement may be of the order of the drag increments sought. However, the zero-angle-of-attack-drag results presented in reference 2 for tests of a similar series of nose shapes show that the drag curves for the various noses at a Mach number of 1.60 fall in much the same order as those of figure 10. This, as well as the lack of scatter exhibited in figure 10, indicates that the drag accuracy is substantially better than is given by a detailed mathematical analysis of the possible errors.

The data indicate that at low lift coefficients, the configuration with the spherical nose produced the greatest drag and showed a difference in drag coefficient of the order of 0.01 (based on wing area) over that for the parabolic-nose configuration, which produced the least drag. It is indicated that the drag for the conical-nose configuration is comparable to that for the parabolic-nose configuration at moderate and high lift coefficients. It appears that the slotted-cone and cone-spike noses are comparable in drag up to. a lift coefficient around 0.3, with the drag curves of these two configurations falling about midway between those for the parabolic- and spherical-nose configurations. The drag reduction effected by the addition of the plain spike seems to have diminished rapidly above an angle of attack of 5° $\left(C_L \approx 0.15\right)$.

Figure 11 shows lift coefficient plotted against angle of attack and indicates that the installation of the several nose shapes had little or no effect on the lift-curve slope.

CONCLUSIONS

An investigation has been made of the effects of various seeker-nose configurations on the pitching-moment coefficient and horizontal-canard control effectiveness, horizontal-canard hinge-moment coefficient, and lift and drag coefficients of a ram-jet canard missile having 70° delta surfaces with pylon-mounted nacelles attached to the fuselage at 90° to the wing plane. The tests were made at a Mach number of 1.60 and a Reynolds number of 3.83×10^6, based on wing mean aerodynamic chord. The results indicated the following conclusions:

1. Static longitudinal stability was virtually unaffected except in the case of the cruciform-nose configuration at high lift coefficients.

2. No configuration among those tested exhibited a significant difference in horizontal-canard control effectiveness except the cruciform nose.

3. Horizontal-canard hinge moments, C_{h_H}, for the conical, slotted-cone, and parabolic-nose configurations were virtually the same. For the spike-nose configurations, C_{h_H}, exhibited a tendency to larger negative moments, the effect being more pronounced for the cone spike.

4. The parabolic-, conical-, slotted-cone, cone-spike, and plain-spike-nose configurations showed less drag at low lift coefficients than the configuration with the spherical nose.

5. None of the nose shapes tested appreciably affected the lift-curve slope.

Langley Aeronautical Laboratory,
    National Advisory Committee for Aeronautics,
        Langley Field, Va., August 26, 1953.

REFERENCES

1. Moeckel, Wolfgang E.: Flow Separation Ahead of a Blunt Axially Symmetric Body at Mach Numbers 1.76 to 2.10. NACA RM E51I25, 1951.

2. Piland, Robert O.: Preliminary Free-Flight Investigation of the Zero-Lift Drag Penalties of Several Missile Nose Shapes for Infrared Seeking Devices. NACA RM L52F23, 1952.

3. Jones, Jim J.: Flow Separation From Rods Ahead of Blunt Noses at a Mach Number 2.72. NACA RM L52E05a, 1952.

4. Beastall, D., and Turner, J.: The Effect of a Spike Protruding in Front of a Bluff Body at Supersonic Speeds. TN No. Aero. 2137, British R.A.E., Jan. 1952.

5. Mair, W. A.: Experiments on Separation of Boundary Layers on Probes in Front of Blunt-Nosed Bodies in a Supersonic Air Stream. Phil. Mag. ser. 7, vol. 43, no. 342, July 1952, pp. 695-716.

6. Platou, A. S.: Body Nose Shapes for Obtaining High Static Stability. Memo. Rep. 592, Ballistic Res. Labs., Aberdeen Proving Ground, Feb. 1952.

7. Hart, Roger G.: Flight Investigation of the Drag of Round-Nosed Bodies of Revolution at Mach Numbers From 0.6 to 1.5 Using Rocket-Propelled Test Vehicles. NACA RM L51E25, 1951.

8. Charters, A. C., and Stein, H.: The Drag of Projectiles With Truncated Cone Headshapes. Rep. No. 624, Ballistic Res. Labs., Aberdeen Proving Ground, Mar. 1952.

9. Spearman, M. Leroy, and Robinson, Ross B.: Wind-Tunnel Investigation of a Ram-Jet Canard Missile Model Having a Wing and Canard Surfaces of Delta Plan Form With 70° Swept Leading Edges: Longitudinal and Lateral Stability and Control Characteristics at a Mach Number of 1.60. NACA RM L52E15, 1952.

10. Hamilton, Clyde V., Driver, Cornelius, and Sevier, John R., Jr.: Wind-Tunnel Investigation of a Ram-Jet Missile Model Having a Wing and Canard Surfaces of Delta Plan Form With 70° Swept Leading Edges: Force and Moment Characteristics of Various Combinations of Components at a Mach Number of 1.6. NACA RM L53A14, 1953.

11. Snow, O. J.: The Development of Irdomes. Progress Rep. Oct. 1, 1950
    to June 1, 1951. Rep. No. NADC-EL-5107, Bur. Aero. TED Project
    No. ADS EL-889, Aeronautical Electronic and Electrical Lab., U. S.
    Naval Air Dev. Center, Oct. 11, 1951.

TABLE I.- GEOMETRIC CHARACTERISTICS OF MODEL WITH PARABOLIC NOSE

Body:

Maximum diameter, in. 2.666
Length, in. 50.833
Fineness ratio 19.067
Base area, sq in. 5.583

Wing:

Span, in. 11.853
Chord at body center line, in. 17.069
Chord at aileron break line, in. 4.606
Area (including that within body), sq in. 104.700
Aspect ratio 1.404
Sweep angle of leading edge, deg 70
Thickness ratio at body center line 0147
Thickness ratio at aileron break line 0543
Leading-edge angle normal to leading edge, deg 15.6
Mean aerodynamic chord, in. 11.48

Aileron:

Area, sq in. 3.201
Mean aerodynamic chord, in. 3.071

Horizontal canards:

Area (exposed), sq in. 6.406
Mean aerodynamic chord, in. 2.576

Vertical canards:

Area (exposed), sq in. 3.203
Mean aerodynamic chord, in. 1.821

NACA

TABLE II.- BODY COORDINATES WITH PARABOLIC NOSE

Body Station	Radius
0	0
.297	.076
.627	.156
.956	.233
1.285	.307
1.615	.378
1.945	.445
2.275	.509
2.605	.573
2.936	.627
3.267	.682
3.598	.732
3.929	.780
4.260	.824
4.592	.865
4.923	.903
5.255	.940
5.587	.968
5.920	.996
6.252	1.020
[a]6.583	1.042
[a]11.542	1.333
[a]50.833	1.333

[a]All contours are straight-line elements between stations noted.

NACA

TABLE III.- NACELLE GEOMETRY
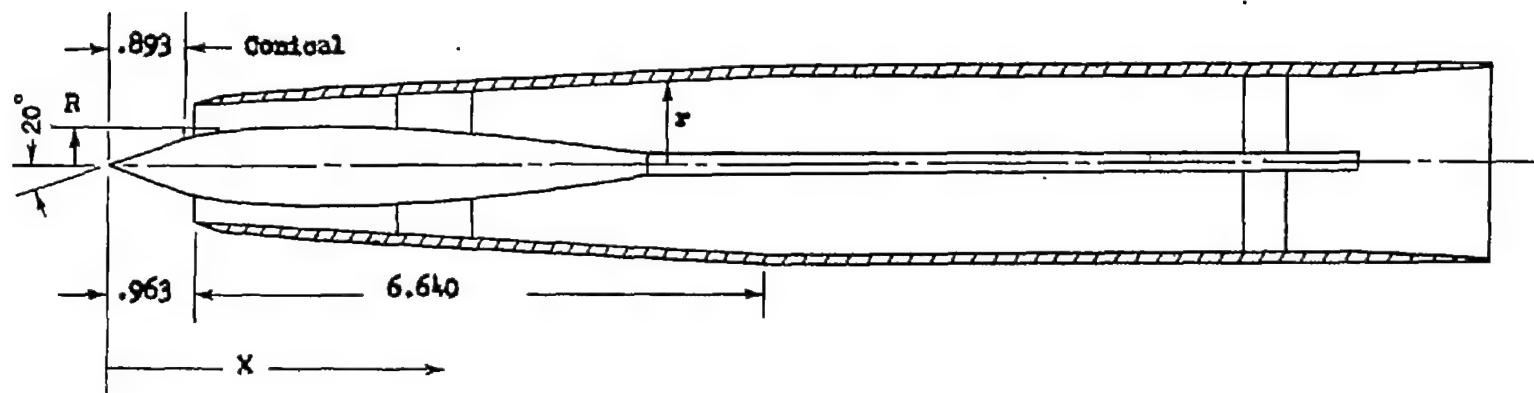
X, in.	R, in.	X, in.	r, in. (a)
0	0		
.893	.325	0.963	0.706
1.000	.360	7.603	.996
1.167	.402	13.712	.996
1.333	.429	14.962	1.069
1.375	.433		
1.500	.441		
1.667	.443		
2.333	.418		
3.000	.375		
6.208	.157		

[a] All internal contours are straight surfaces between the points noted.
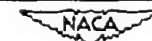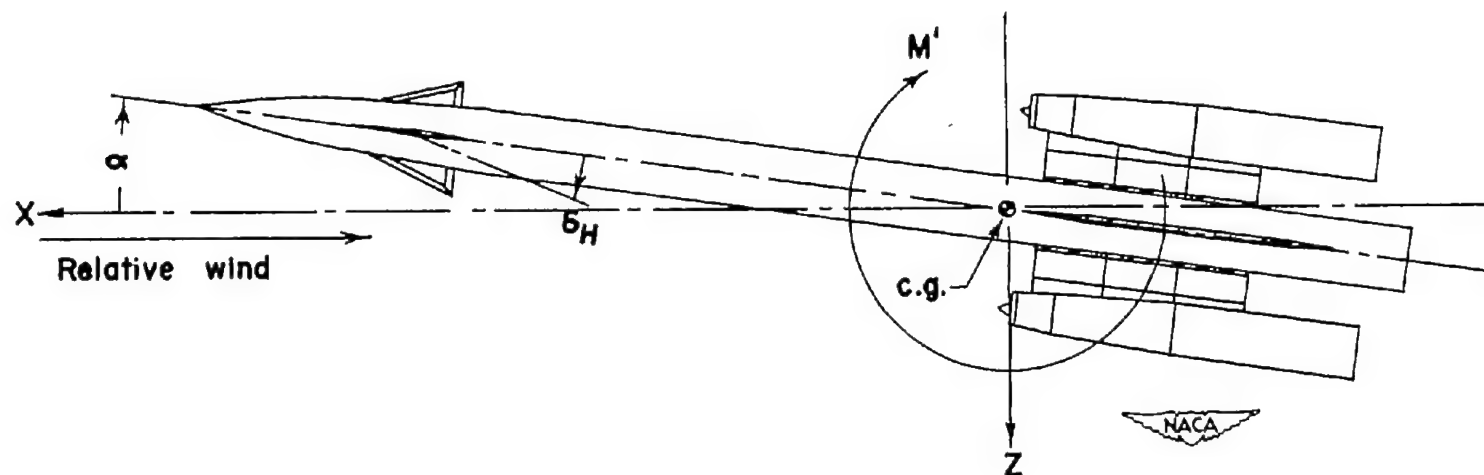
Figure 1.- System of longitudinal stability axes. Arrows indicate
positive values.
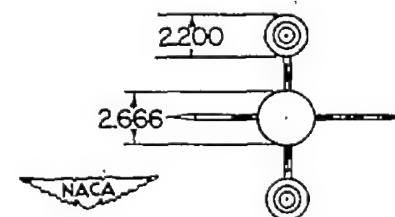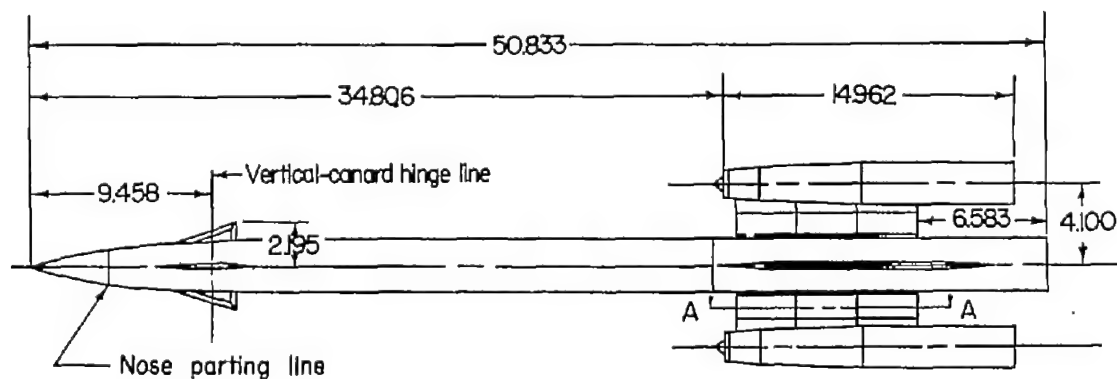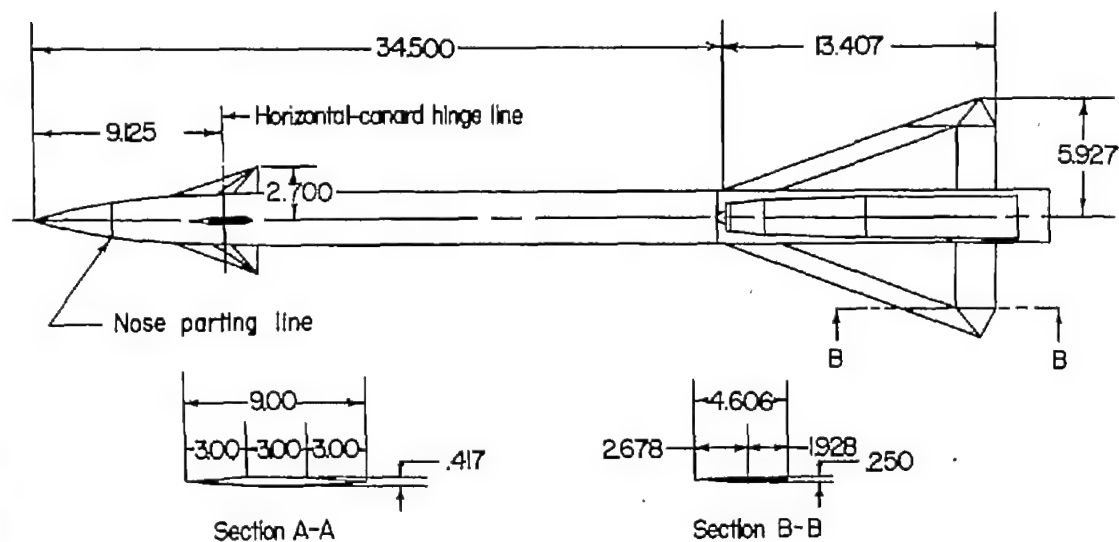
Figure 2.- Details of ram-jet canard missile model. All dimensions are in inches.
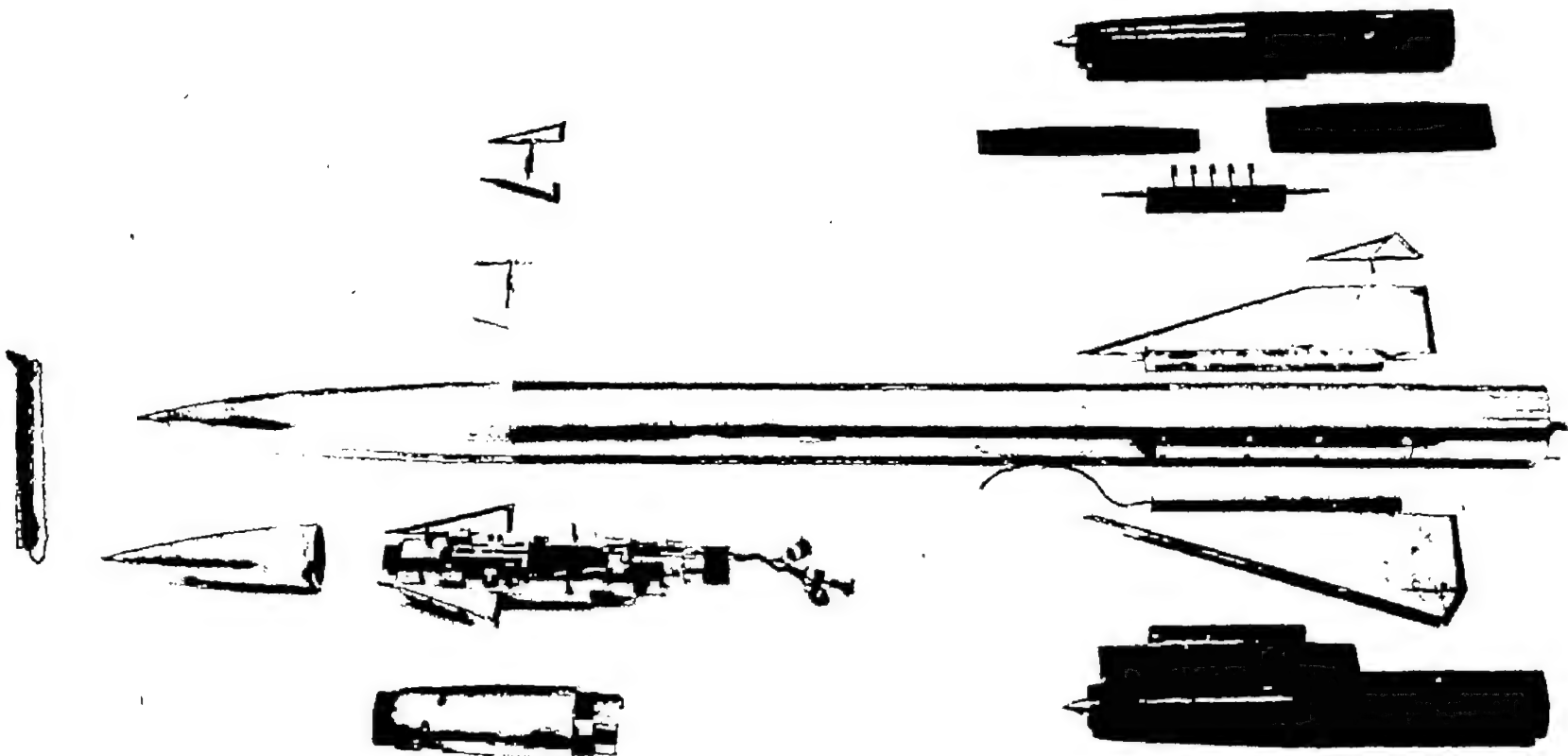
Figure 3.- Photograph of model components.

L-74957
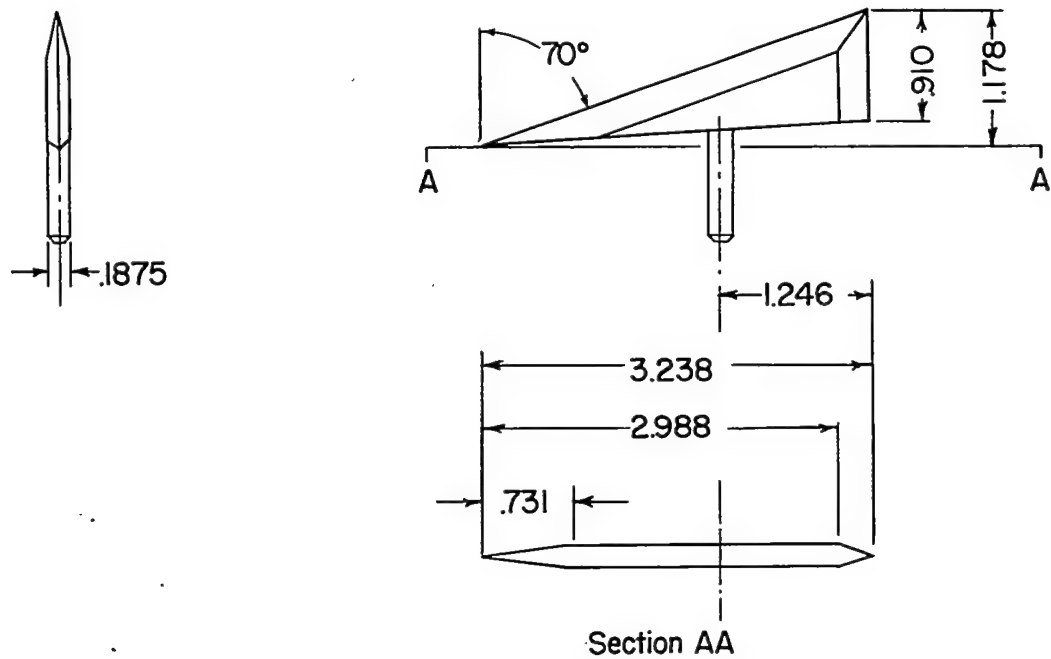
(a) Vertical canard.
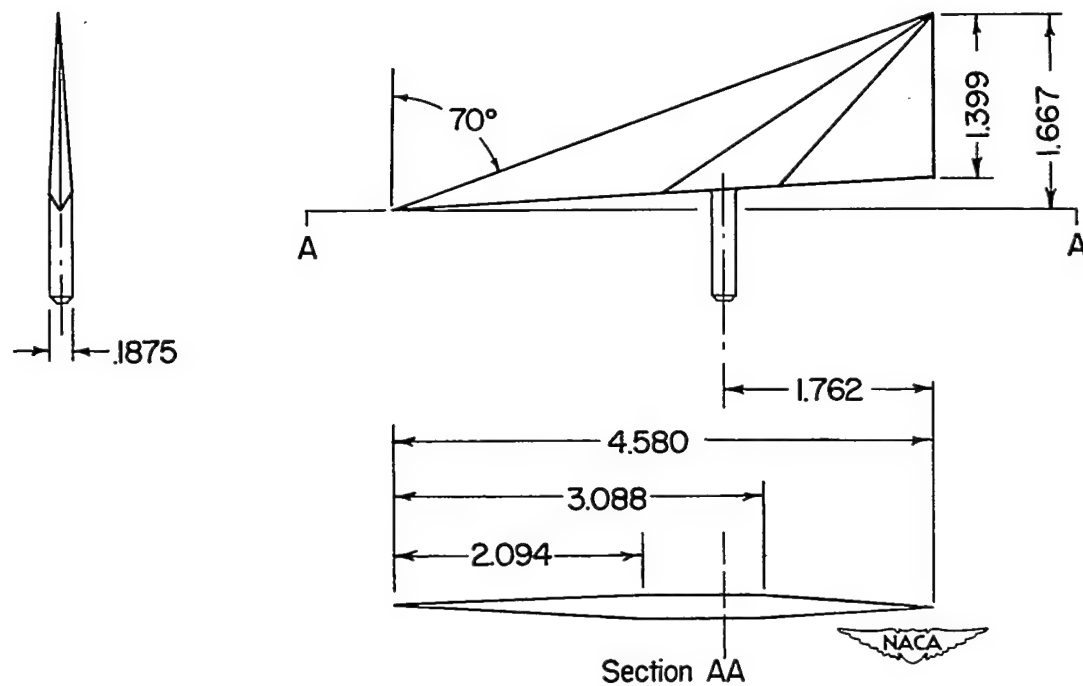
(b) Horizontal canard.

Figure 4.- Details of control surfaces and wing. All dimensions are in inches.

.250

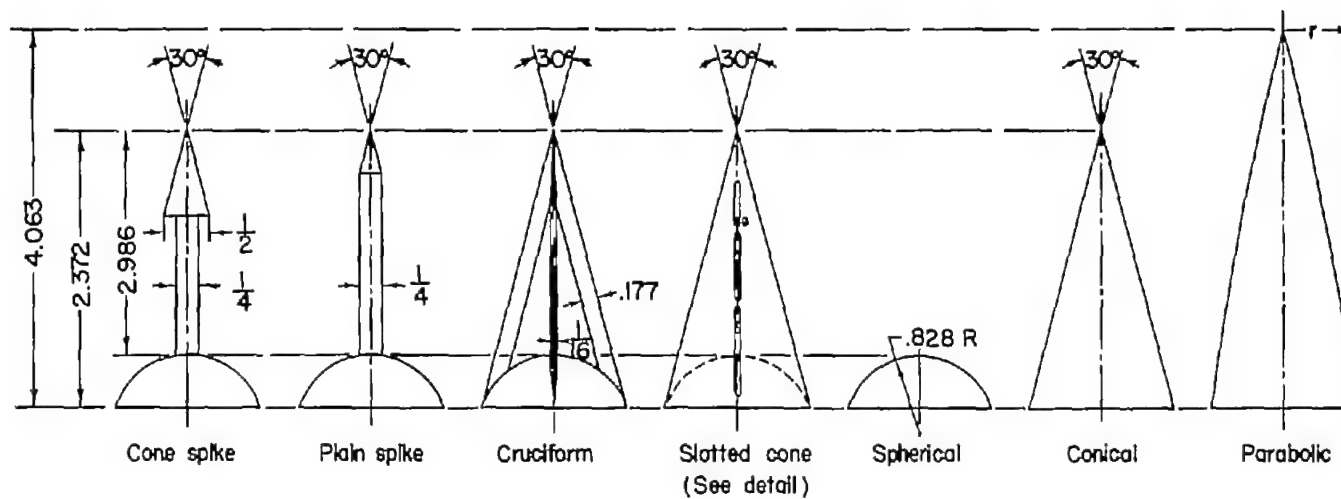Wing section at body juncture

Wing area enclosed by body

.0005

1.390

.803

4.606

.250

Wing section at gap

.184

Aileron section at gap
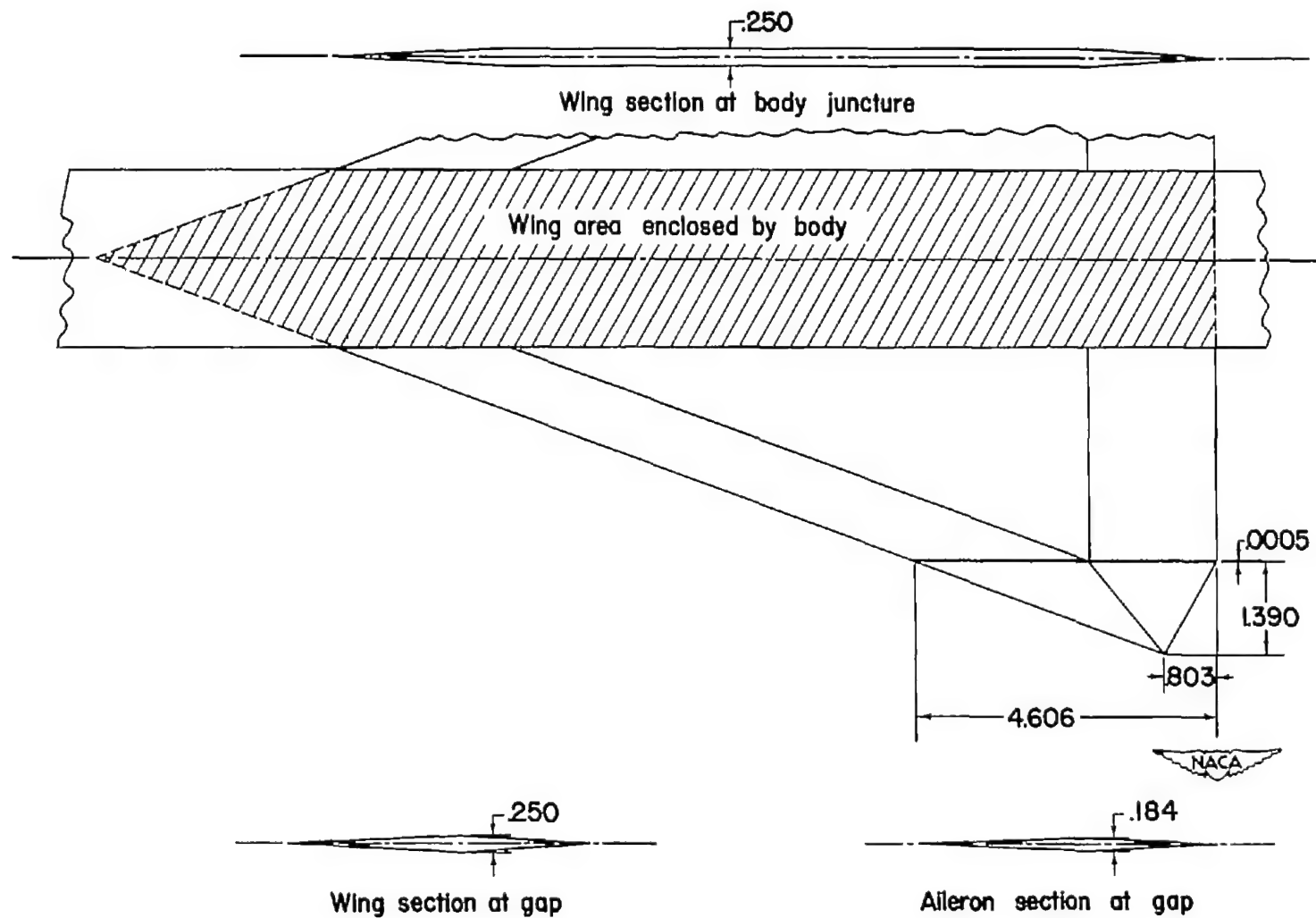
(c) Aileron and wing details.

Figure 4.- Concluded.

Top view of Installation

Side view of Installation

8.249

11.703

4.500

Sting

Body

NACA
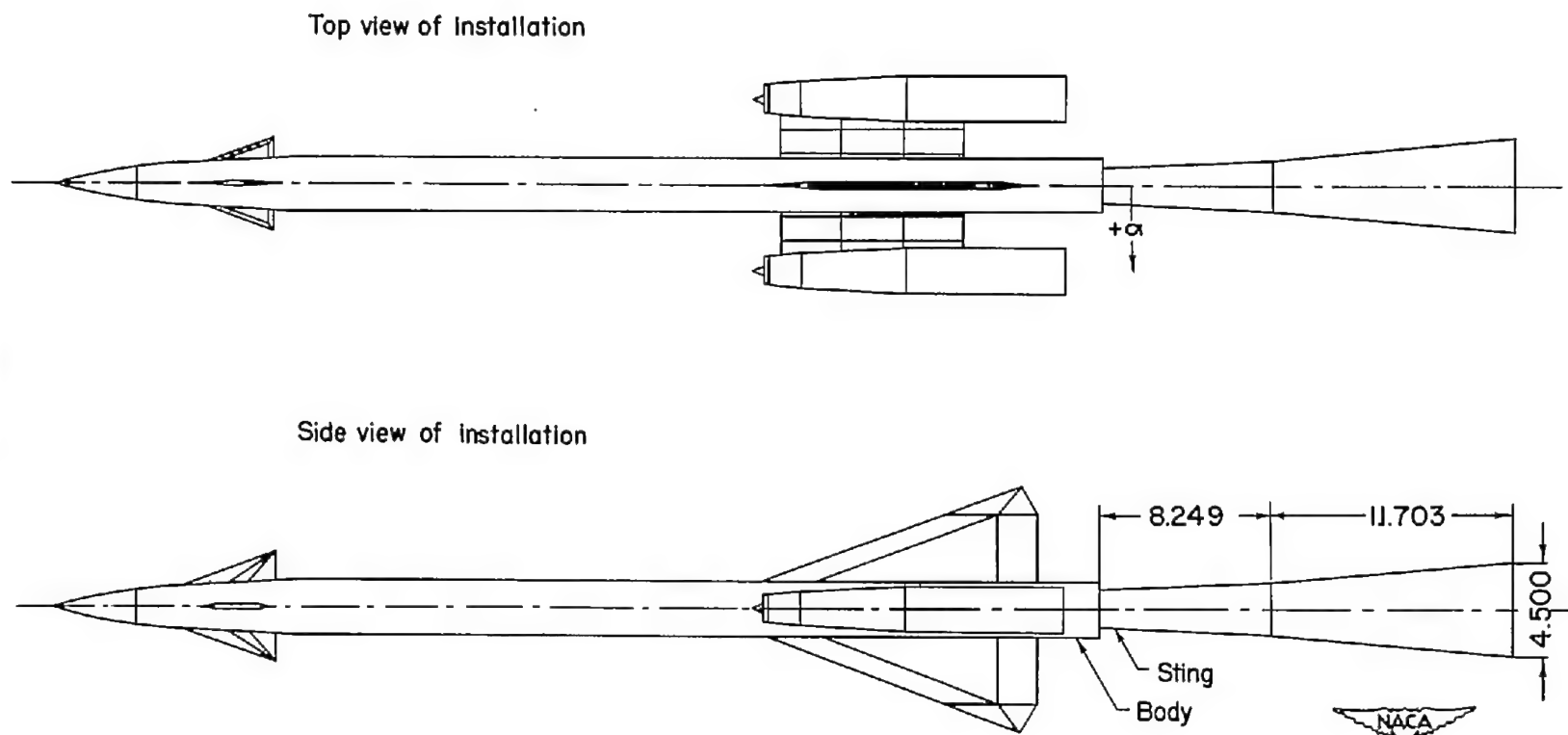
Sting diameter at model base   1.890

Figure 5.- Details of model installation. All dimensions are in inches.
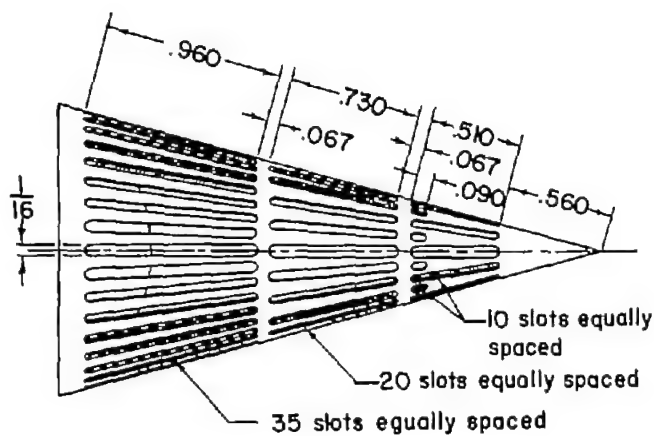
Slotted-cone details

Parabolic-nose coordinates

Body station, x	Radius, r
0	0
.297	.076
.627	.156
.956	.233
1.285	.307
1.615	.378
1.945	.445
2.275	.509
2.605	.573
2.936	.627
3.267	.682
3.598	.732
3.929	.780
4.063	.800

Figure 6.- Details of nose shapes. All dimensions are in inches.
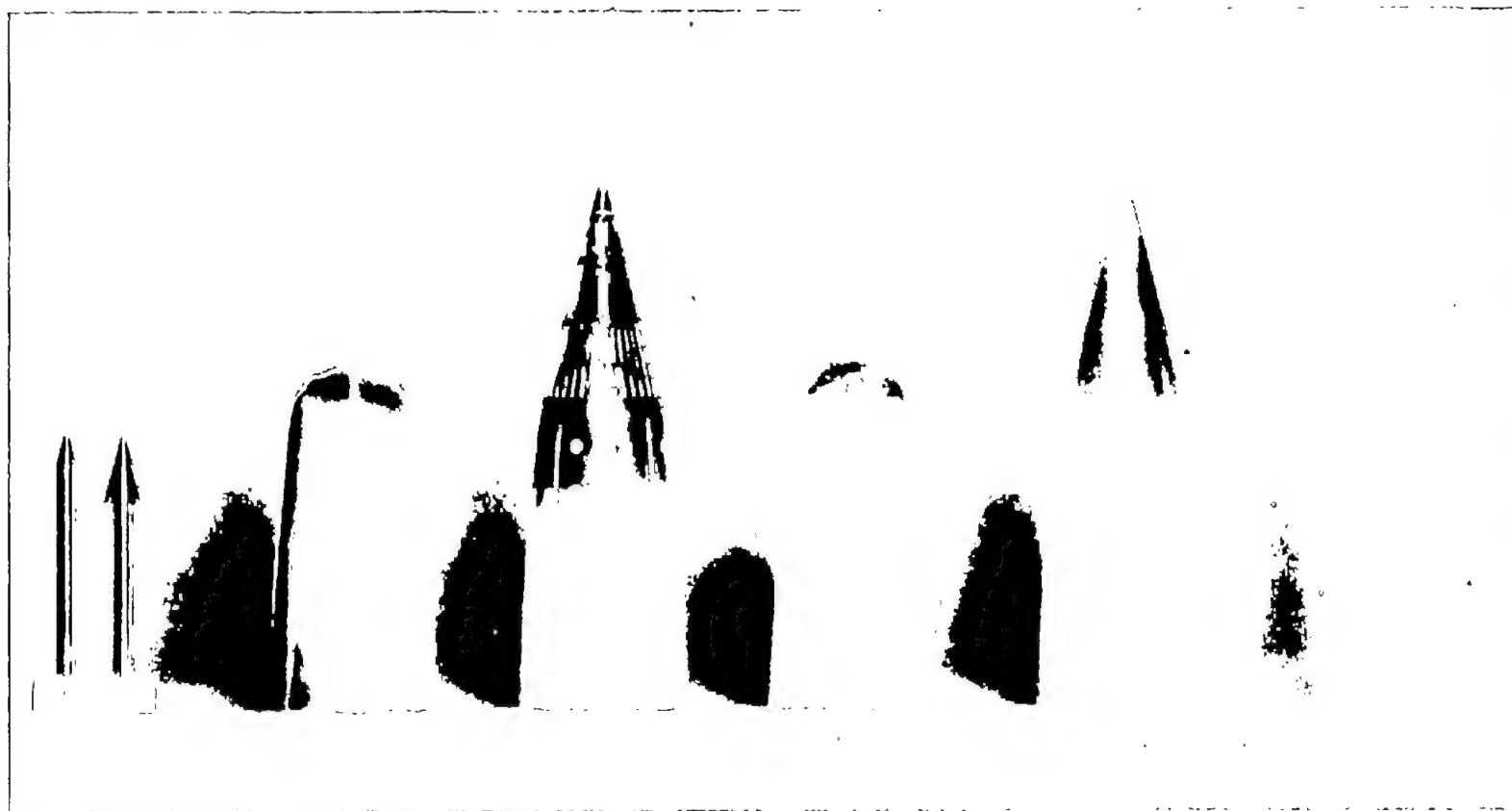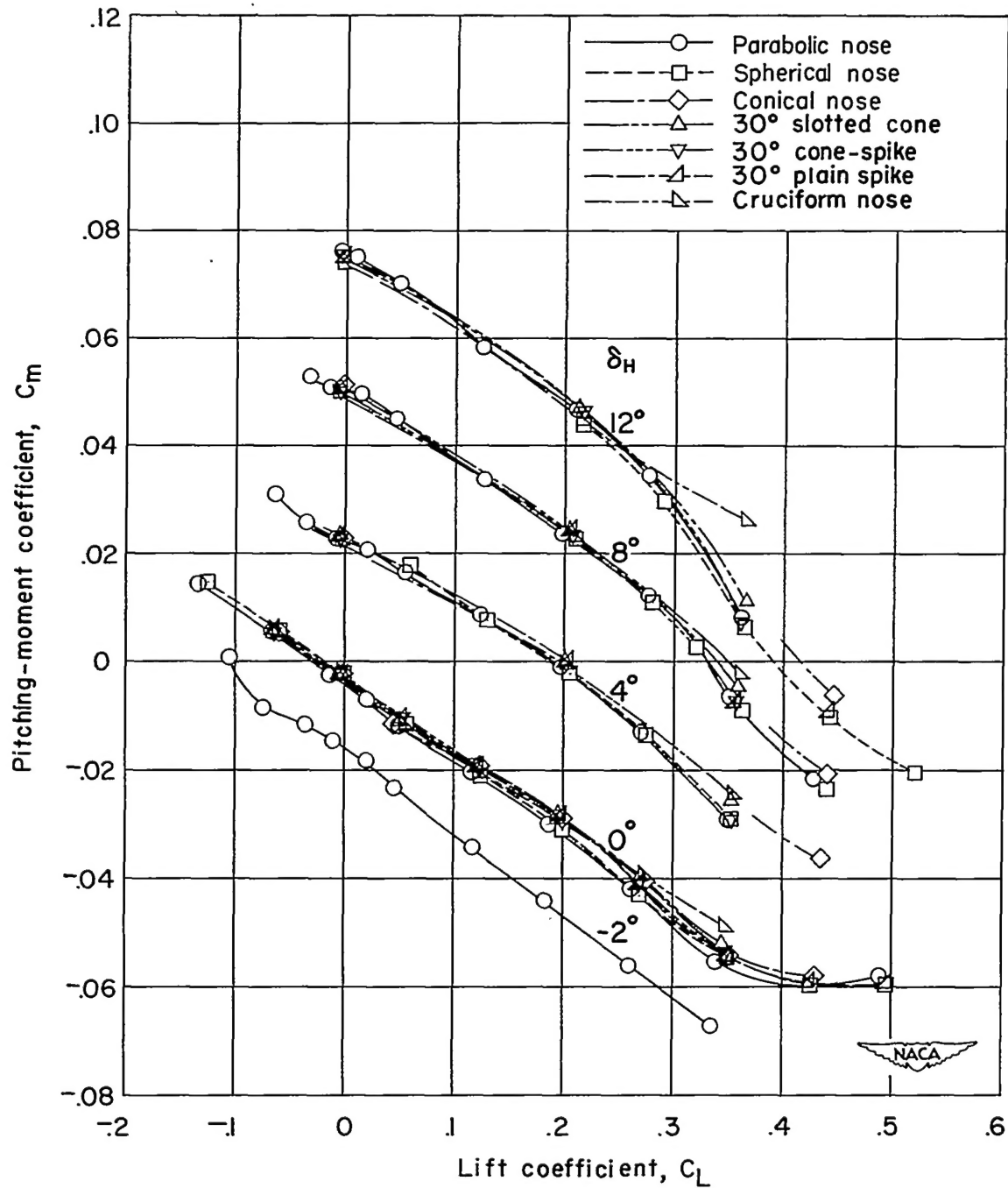
L-80573

Figure 7.- Nose configurations.

Figure 8.- Variation of pitching-moment coefficient with lift coefficient
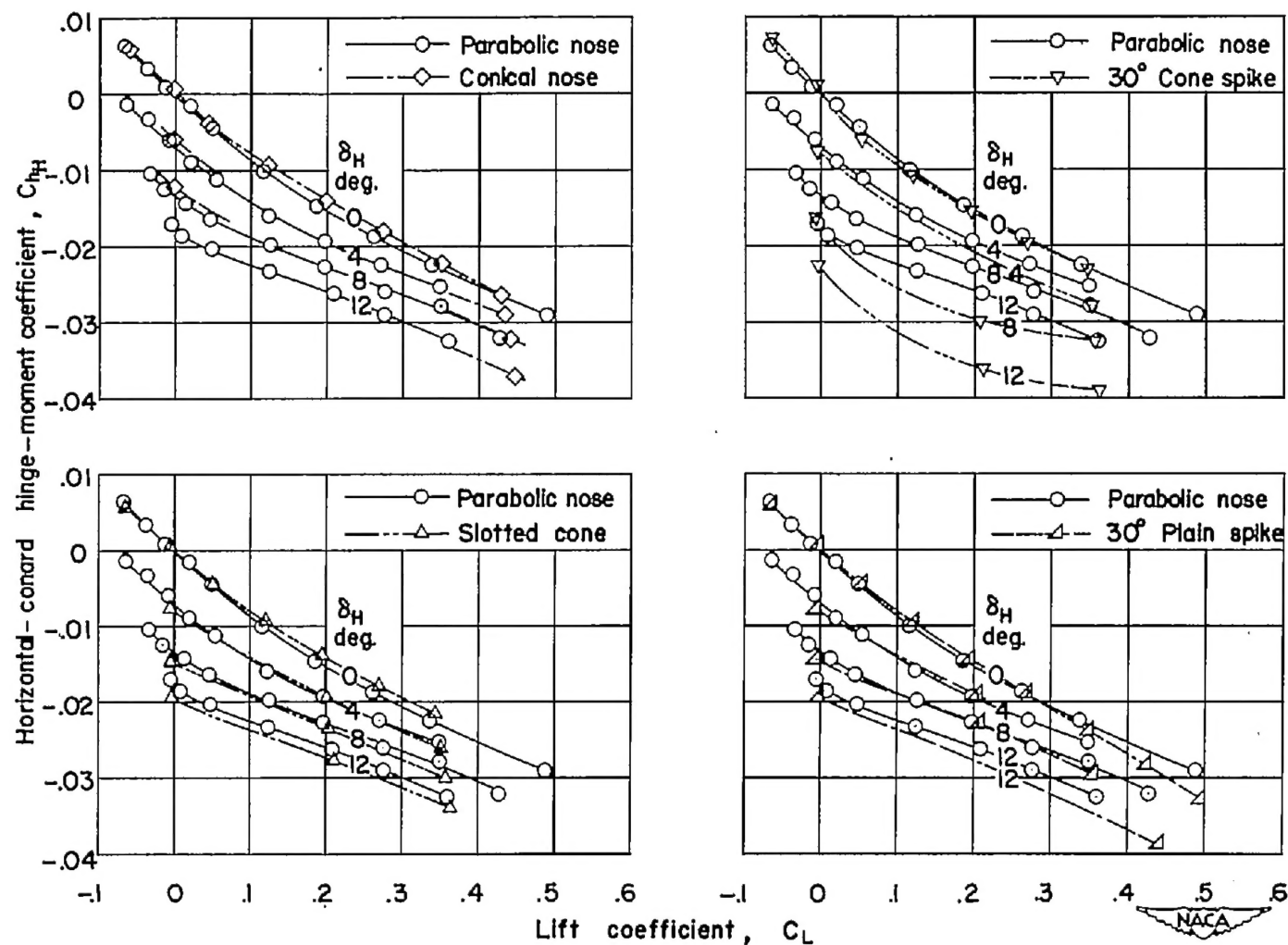for various values of horizontal-canard deflection and various nose
shapes.

Figure 9.- Variation of horizontal-canard hinge-moment coefficient with lift coefficient at various horizontal-canard deflections for several nose shapes as compared to original parabolic nose.
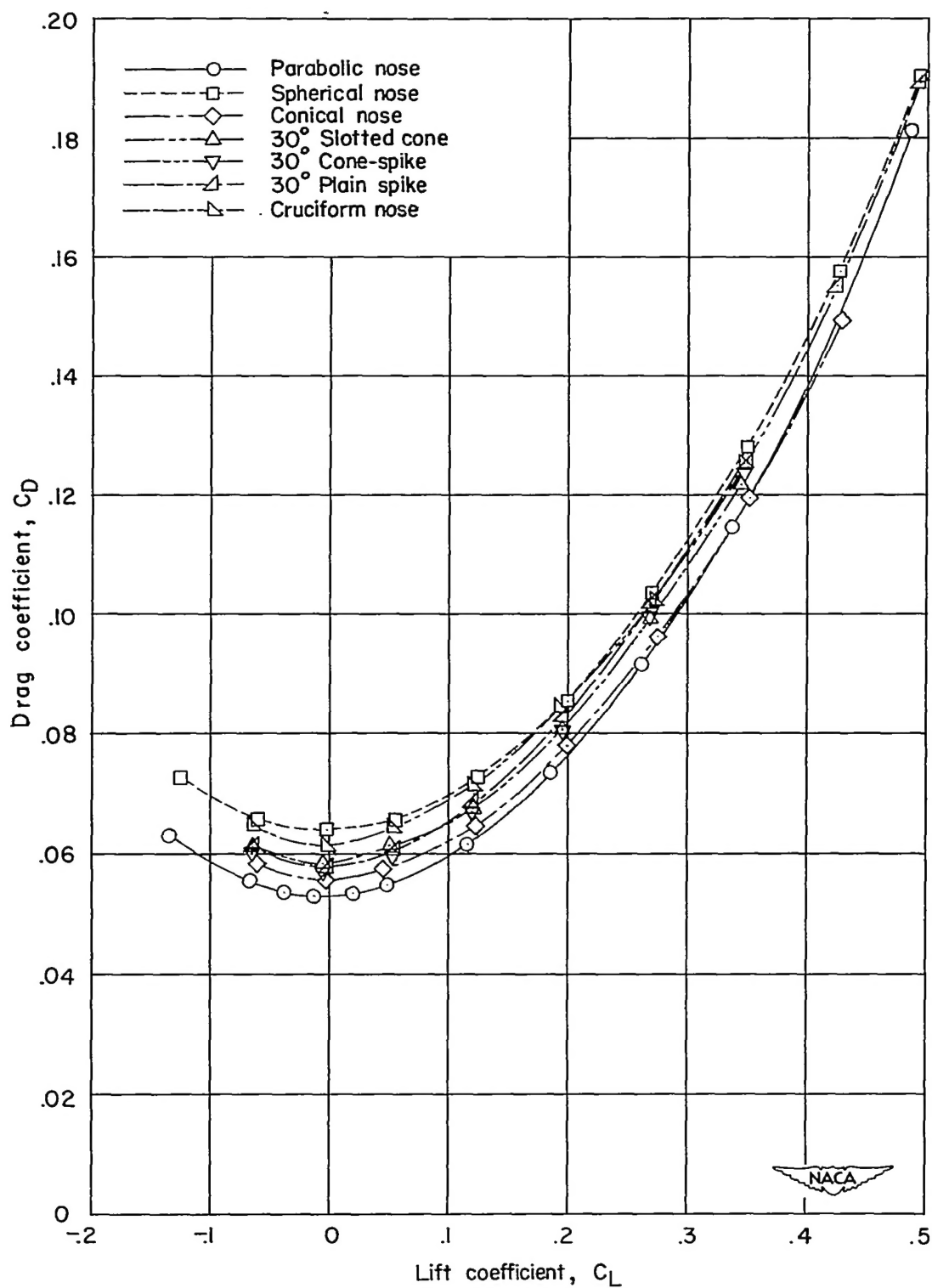
Figure 10.- Variation of drag coefficient with lift coefficient at $\delta_H = 0$ for various nose shapes.
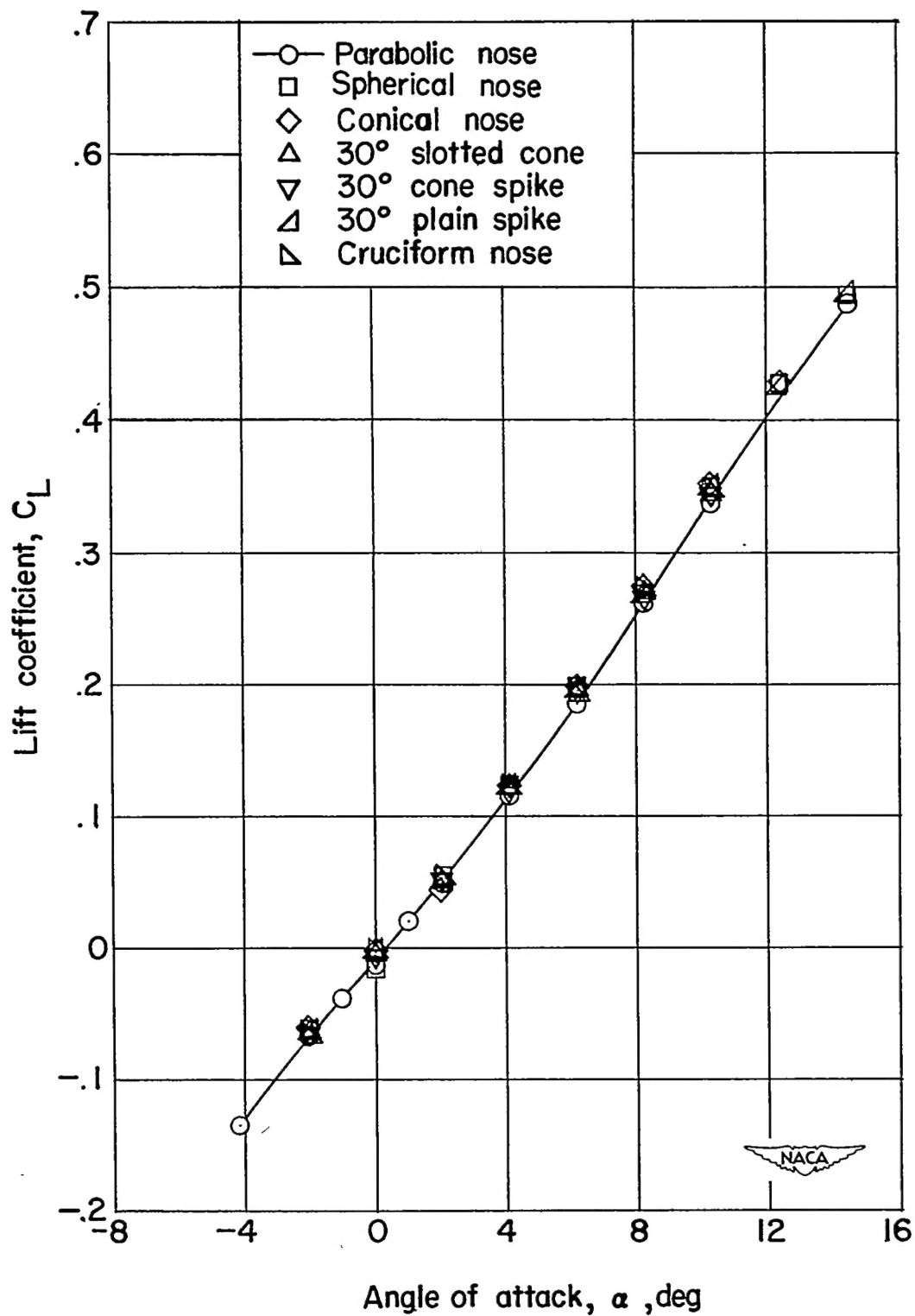
Figure 11.- Variation of lift coefficient for $\delta_H = 0$ with angle of attack for various nose shapes.